RSC Advances

PAPER

View Article Online
View Journal | View Issue

Cite this: *RSC Adv.*, 2023, **13**, 25437

Modified graphene foam as a high-performance catalyst for oxygen reduction reaction†

Malgorzata Skorupska, *[a] Anna Ilnicka [a] and Jerzy P. Lukaszewicz[ab]

Received 22nd June 2023
Accepted 21st August 2023

DOI: 10.1039/d3ra04203k

rsc.li/rsc-advances

Gelatine and chitosan were used as natural precursors for nitrogen-doping of the graphene foam structure, creating specific types of active sites. The quantitative and qualitative content of nitrogen groups in the carbon structure was determined, which, under the influence of high temperature, were incorporated and transformed into forms of functional groups favorable for electrochemical application. Electrochemical studies proved that the form of pyridine-N, pyrrole-N, and quaternary-N groups have favorable electrochemical properties in the oxygen reduction reaction comparable to commercial platinum-based electrode materials. Using these materials as electrodes in metal–air batteries or fuel cells may eliminate the use of noble metal-based electrodes.

Introduction

Presently, there is an urgent need to minimize environmental pollution and find sustainable technology for energy production, storage and conversion. All this is due to the growing industry, whose demand for energy is constantly increasing. Over the past few decades, energy storage devices have become the focus of much attention, fuelling rapid progress in the development of electrode materials for devices such as fuel cells and metal–air batteries. Researchers are continually improving current electrocatalysts to make them more environmentally friendly, improve their conductive properties, and efficiency by refining their electrochemical properties. Currently, commercially available electrocatalysts contain noble metals such as platinum, iridium, or ruthenium. Platinum has excellent oxygen reduction reaction (ORR) activity, but the disadvantages are its price and limited sources. From an economic and environmental point of view, noble metal-free electrocatalysts are a noteworthy alternative. The properties that such an electrocatalyst should have are good conductivity, a large specific surface area (SSA), and the absence of noble metals in the structure.[1,2] Graphene and the doping of heteroatoms of the graphene structure with elements such as nitrogen sulphur, boron or phosphorus play a good role in this respect.[3–7] When constructing new electrocatalysts, carbon materials can act directly in the oxygen reduction reaction *via* active sites in the structure, making them an effective energy carrier.[8] Various conductive natural and synthetic polymers are used to enhance the catalytic properties, expand the surface conductive properties or introduce heteroatoms into the structure. The polymeric matrix precursors involved in the synthesis of 3D hybrid materials to date include polymethylmethacrylate, sulfonated polystyrene, and poly(vinylpyrrolidone) beads,[9,10] polyurethane or polydimethylsiloxane,[11] polycaprolactone.[12] Poly(ethylene mine), polyaniline, and polypyrrole have been used as nitrogen precursors.[13,14] Natural polymers include cellulose,[15] starch,[16] wood[17] and also gelatine and chitosan.[18] These polymers are mainly used to improve the properties of carbon materials for biomedical applications. The degree of oxidation of polymers and their stability is very important in energy storage devices.[19] However, in the case of natural polymers, no use has been found for the synthesis of electrode materials for oxygen reduction reactions. The natural polymers are promising alternative to expensive carbon precursors and their use in combination with graphene, can give materials with advanced electrochemical properties.

Despite the observed progress in the synthesis of Pt-free ORR catalysts, some domains still need to be explored. In particular, the application of natural precursors is of interest. If properly selected, natural precursors may ensure the instant transfer of N atoms to carbon matrices upon carbonization of such precursors. If carbonized solely, some natural precursors are transformed into carbon matrices of relatively low electric conductivity unless the carbonization temperature exceeds 800–900 °C. On the other hand, high carbonization temperatures lead to the collapse of pores and diminishing structural parameters such as specific surface area and the total pore volume. In parallel, the N-content also decreases due to the release of volatile species that contain nitrogen at higher temperatures.

[a]*Faculty of Chemistry, Nicolaus Copernicus University in Torun, Gagarina 7, 87-100 Torun, Poland. E-mail: m.skorupska@doktorant.umk.pl*

[b]*Centre for Modern Interdisciplinary Technologies, Nicolaus Copernicus University in Torun, Wilenska 4, 87-100 Torun, Poland*

† Electronic supplementary information (ESI) available: Synthesis and characterization techniques data. Additional electrochemical data. See DOI: https://doi.org/10.1039/d3ra04203k

As mentioned in earlier literature reports, it is true that nitrogen doping increases defects in the structure of graphene, which can be observed by analyzing Raman spectroscopy. The intensity of the D-band indicates a defected structure of the material. As described in an earlier literature review[20] the interaction between nitrogen and the neighboring carbon is significant. The introduction of nitrogen into the sp^2 carbon structure alters the electronic properties of the carbon atoms due to the higher electronegativity of nitrogen. The activity is attributed to the different nitrogen functional groups and, as assumed, with increasing heat treatment temperature, N pyrrole transforms into N pyridine and N quaternary.[21,22] However, indirect factors such as the morphology of the carbon materials must also be taken into account. An appropriate correlation between surface area and oxygen availability and the content of the corresponding functional group can improve the catalytic properties. In the case of the research described in this manuscript, the calculated electron transfer value is indicative of a four-electron pathway which is influenced by a component of all the factors described above. In the present work, we attempt to resolve the problem caused by the mentioned contradictions. Graphene and widely available natural polymers gelatine and chitosan were used low-cost precursors to obtain N-doped graphene foams with porous structure. The effect of the carbonization temperature on the content of nitrogen functional groups and catalytic properties was investigated. The best oxygen reduction properties in the alkaline medium are exhibited in materials carbonized at 800 °C. Several instrumental analyses were performed for broad characterization. Among others, a high-resolution transmission electron microscope was used to determine the structure and morphology of the graphene foams. To the best of our knowledge, it is the first report on the aggregate use of graphene and natural polymers to obtain N-doped graphene foams for practical application in oxygen reduction reaction.

Materials and methods

The N-doped graphene foams were synthesized based on the synthesis stages presented in Scheme S1.† The commercial graphene nanoplatelets (GNPs) were used as the carbon source, and gelatine or chitosan was used as the nitrogen source and the medium for hydrogel formation. In the first series (1F), gelatine and Na_2CO_3 (16.9% w/v) were dissolved in 20 ml of distilled water, heated and stirred continuously to dissolve the reagents completely. The GNPs were added to the clear solution while stirring continuously and then left to stand until the next day. The ratio of gelatine to GNPs was 2.5 : 1. Then 0.5 g of instant yeast was added to the mixture and stirred, followed by 10 ml of perhydrol (30%). Yeast and perhydrol were used in the reaction to form the foamed structure. The yeast acted as a catalyst for the decomposition of perhydrol into water and oxygen, thus accelerating the decomposition process and keeping the oxygen molecules in a dense matrix. In the second series (2F), the chitosan material was prepared the same way as in series 1F except that a solution consisting of 10 ml H_2O/1 ml HCl was added to gel the chitosan. In both series, 1F and 2F samples were freeze-dried to remove water from the foam. After the freeze-drying process, the samples were carbonized in an N_2 atmosphere at 600, 700, 800, or 900 °C with a heating rate of 3 °C min^{-1} and a holding time of 1 hour. The samples obtained after the carbonization process were washed with hydrochloric acid to remove all unreacted substrates and then with distilled water to a neutral pH. They were dried at 110 °C in an electric dryer until completely dry. N-doped graphene foams synthesized with gelatine were denoted as 1F_*T*, where *T* is carbonization temperature 600 °C, 700 °C, 800 °C, 900 °C, respectively. The second series of N-doped graphene foams obtained with chitosan were denoted as 2F_*T*.

The materials were used for the synthesis and the synthesis scheme are described in the ESI.† A description of the techniques used to characterize the materials and electrochemical measurements are also described in the ESI.†

Results and discussion

Materials characterization

The morphology was investigated by high-resolution transmission electron microscopy (HRTEM) analysis. The HRTEM images at various magnifications show the resulting N-doped graphene foams presented in Fig. 1 and S1.†

For samples 1F_800 and 2F_800, a wrinkled structure is observed and also consisted of several overlapping individual graphene layers. The distance between individual graphene layers is within the range of literature data and is 0.35 nm.[23] Such an extended structure and uneven edges, is characteristic of N-doped graphene foams.

The elemental composition of carbon, nitrogen, and hydrogen is summarized in Table 1. For electrochemical application, nitrogen concentration, in particular, will play an important role in the oxygen reduction reaction; therefore, optimizing their concentration is essential.[24] Notably, it is possible to control the limiting current density and effectively use the heteroatoms incorporated into the structure to reduce the overpotential.[25,26] For the 1F_*T* series, the percentage of nitrogen content decreases from 6.39 wt% to 2.39 wt% with an increase in the carbonization temperature from 600 to 900 °C, respectively. The second series of 2F_*T* N-doped graphene foams showed the same trend with a decrease in nitrogen content from 5.72 wt% to 2.43 wt%. This is a typical trend for non-permanent nitrogen groups, which undergo a decomposition process at higher temperatures resulting in a decrease in the total nitrogen content of the materials obtained.[1] In the case

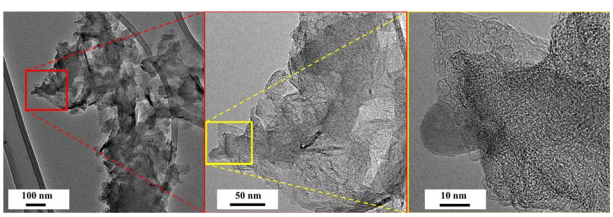

Fig. 1 High-resolution transmission electron microscopy images of 1F_800 sample at different magnifications.

Table 1 Elemental content of C, H and N elements determined by combustion analysis, porosity parameters, and intensity ratios of G, D, and 2D-bands from the Raman spectra of 1F_*T* and 2F_*T* series[a]

Sample	Elemental content (wt%)			S_{BET}	V_t	V_{mi}	V_{me}	I_D/I_G	I_{2D}/I_G
	C	H	N						
GNPs	87.32	0.90	0.72	750	0.99	0.13	0.86	0.64	0.40
1F_600	79.61	1.84	6.39	453	0.44	0.14	0.30	0.99	0.30
1F_700	83.54	1.63	3.93	768	0.64	0.22	0.42	1.01	0.27
1F_800	88.75	1.33	2.86	861	0.77	0.21	0.56	0.81	0.30
1F_900	96.07	0.97	2.39	795	0.77	0.17	0.61	0.90	0.32
2F_600	76.91	2.32	5.72	287	0.34	0.07	0.28	0.90	0.28
2F_700	78.74	1.41	5.16	648	0.51	0.18	0.32	0.99	0.27
2F_800	81.88	1.97	3.39	769	0.56	0.23	0.32	1.03	0.32
2F_900	93.65	0.93	2.43	941	0.64	0.29	0.35	0.94	0.25

[a] S_{BET} – ($m^2\ g^{-1}$), V_t – ($cm^3\ g^{-1}$), V_{mi} – ($cm^3\ g^{-1}$), V_{me} – ($cm^3\ g^{-1}$).

of the carbon content for 1F_*T* and 2F_*T* series, their concentration increase from 79.61 wt% to 96.07 wt% and 76.91 wt% to 93.65 wt% with the increase of carbonization temperature. This relationship is typical for carbonaceous materials as the number of carbon bonds increases with increasing temperature, causing an increase in the degree of graphitization.

The porosity of the obtained N-doped graphene foams was determined by sorption of nitrogen analysis. Fig. S2a and b† present adsorption–desorption isotherms of the materials obtained in 1F_*T* and 2F_*T* series and commercial GNPs. The shape of curves for the obtained samples are characteristic of type-II isotherm with a visible hysteresis loop according to the IUPAC classification.[27] The SSA was calculated by Brunauer–Emmett–Teller (BET) equation and compared with commercial graphene in Table 1. In the 1F_*T* series, the sample carbonised at 800 °C has the highest SSA, 861 $m^2\ g{-}^1$. The specific surface area of samples 1F_600, 1F_700 and 1F_900 is 453 $m^2\ g^{-1}$, 768 $m^2\ g{-}^1$ and 795 $m^2\ g{-}^1$, respectively. The decrease in surface area for sample 1F_900 relative to 1F_800 may be due to the collapse of the structure during the intense release of gaseous thermal transformation products. Similar trend was observed for materials obtained from gelatine by Yang *et al.*[28] The 2F_*T* series showed a trend of increasing SSA with increasing carbonization temperature. The obtained material 2F_600 carbonized at 600 °C shows the lowest specific surface area of 287 $m^2\ g{-}^1$. The 2F_900 sample carbonised at 900 °C has a higher SSA than GNPs of about 191 $m^2\ g^{-1}$. The value of the specific surface area of sample 2F_900 was 941 $m^2\ g^{-1}$. The use of two-dimensional-non localised density functional theory (2D-NLDFT) method permitted the determination of the pore size for the N-doped graphene foams. The subtle differences are shown in Fig. S2c and d.† The pore volumes were compared with commercial graphene and are summarised in Table 1. The pore sizes of the materials in detail is described in the ESI.†

The Raman spectra Fig. 2 possess three characteristic bands, D, G, and 2D. The intensity ratio of the D to G bands and 2D to G bands are shown in Table 1. Explanations of the meaning of

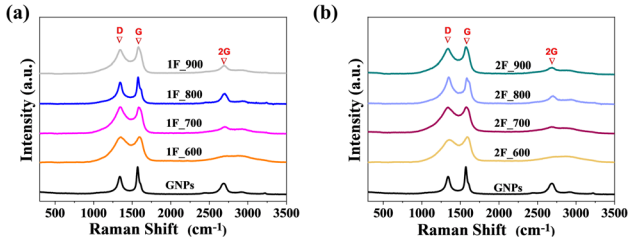

Fig. 2 Raman spectra of samples in series (a) 1F_*T* and (b) 2F_*T* compared to GNPs.

individual peaks and the intensity ratio of D to G bands (I_D/I_G) and 2D to G bands (I_{2D}/I_G) are described in the ESI.†

The type of functional groups in the N-doped graphene foams is very important and influences the catalytic properties. Therefore, X-ray photoelectron spectroscopy (XPS) analysis was used to determine the content of functional groups.

The resulting XPS spectra were taken for 1F_800 and 2F_800 samples. The tests performed made it possible to determine the type of elements present in the XPS survey spectra (Fig. 3a and

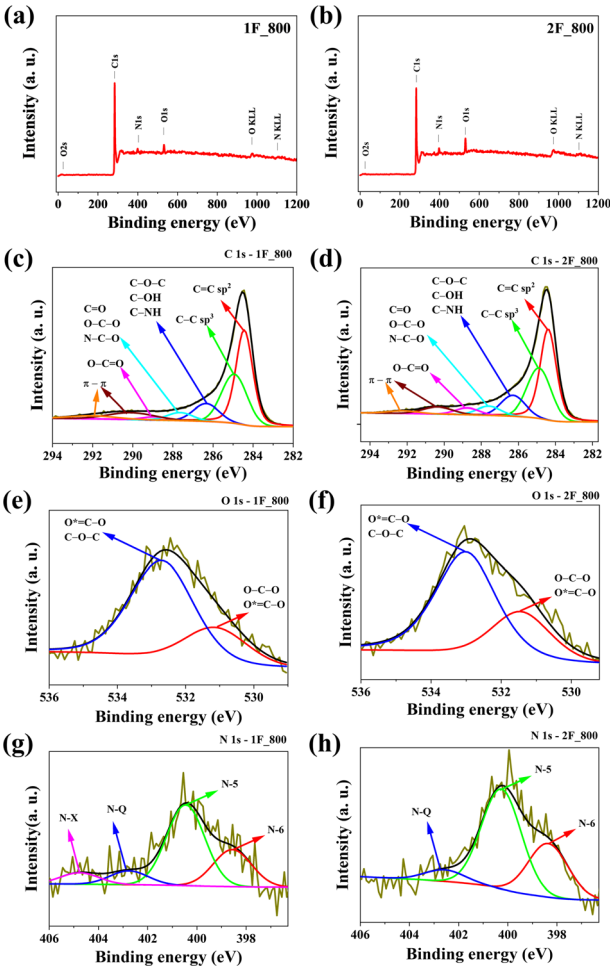

Fig. 3 (a and b) The XPS survey spectra. The high-resolution XPS spectra of (c and d) C 1s, (e and f) O 1s, (g and h) N 1s for 1F_800 and 2F_800 sample.

b). The natural polymers used, gelatine and chitosan, were the sources of carbon and nitrogen atoms. High-resolution spectra were determined for carbon (Fig. 3c and d), oxygen (Fig. 3e and f), and nitrogen (Fig. 3g and h). The individual spectra and corresponding bonds at a given energy value are described in the ESI.† Under the influence of high temperatures, the nitrogen atoms were transformed into the corresponding nitrogen functional groups (Table S1†).

In the literature, researchers described different nitrogen groups responsible for electrochemical activity. In one paper, the authors suggested that pyrrole-N, pyridinic-N and graphitic-N influence activity in the oxygen reduction reaction.[29] In another case, pyridinic-N enhances activity in the oxygen reduction reaction and, in combination with another heteroatom, may also effectively contribute to the use of materials as catalysts for additional application.[30–32]

Electrochemical performance

Catalytic activity is an extremely important parameter when evaluating electrocatalysts determined by cyclic voltammetry (CV) and linear sweep voltammetry (LSV). The potential application of the obtained electrocatalysts was investigated in relation to oxygen reduction reaction, which is a crucial reaction in metal–air batteries or fuel cells. The CV curves (Fig. 4a and S3a†) obtained for both series of materials possess characteristic cathodic peaks, which indicates the catalytic activity of the composites obtained. The cathodic peak for the samples in the 1F_*T* series was in the potential range from 0.77 to 0.80 V *vs.* the reversible hydrogen electrode (RHE). In series 1F, the current density range for sample 1F_800 is the widest, which may indicate high activity over a wide range of current densities. For the 2F_*T* series, a shift of the cathode peak towards positive potential values is evident. The peak range in which oxygen reduction occurs for the samples in the 2F_*T* series is between 0.75 and 0.81 V *vs.* RHE. In series 2F, sample 2F_900 shows the broadest range of current density than the other samples in this series. By analyzing the LSV voltammograms (Fig. 4b and S3b†) and onset potential determined on LSV curves (Fig. 4c and S3c†) at a scan rate of 5 mV s^{-1} and a sweep rate of 1600 rpm, the most effective catalysts in the oxygen reduction reaction can be selected.

Based on the results from the LSV method measured at different speeds in the range from 800 to 2800 rpm, using the equations and the K–L diagram (Fig. 4d and S3d†), the number of electrons involved in the ORR reaction was determined. After calculations determining the number of electrons transferred, it can be concluded that the materials from both series demonstrate a four-electron oxygen reduction pathway (Table 2). Fig. 5 shows the number of electrons involved in the oxygen reduction reaction for samples of 1F_*T* and 2F_*T* series and also for GNPs, and commercial platinum-based catalysts.

Chronopotentiometric tests were carried out to assess the durability of the 1F_800 and 2F_800 electrodes. Stability tests were measured for 5 h at 0.5 V *vs.* RHE. The obtained materials exhibit high durability in the oxygen reduction reaction after 5 h the materials still maintained high current stability, indicating a potential alternative to metal-containing catalytic materials. A graph showing the stability of the best materials is shown in the ESI on Fig. S4.†

Slight differences can be seen in the variation of the carbonization temperature. For the first 1F_*T* series, the number of electrons ranged from 3.16 to 3.88. The highest number close to the four-electron pathway was exhibited by sample 1F_700 at 3.88. Nevertheless, comparing the other parameters, such as current density and diffusion-limiting current, indicates that it is possible to choose the best carbonization temperature for the 1F_*T* series. Therefore, temperatures of 700 °C or 800 °C are required to obtain favorable catalysts synthesized with gelatine. As for the second 2F_*T* series, it is apparent that as the carbonization temperature increases, the electron number also increases, ranging from 3.19 to 3.99. A breakdown of this trend can also be seen for the highest carbonization temperature of 900 °C; for sample 2F_900, the electron number is 3.43. Therefore, the highest electron number involved in the oxygen reduction reaction for

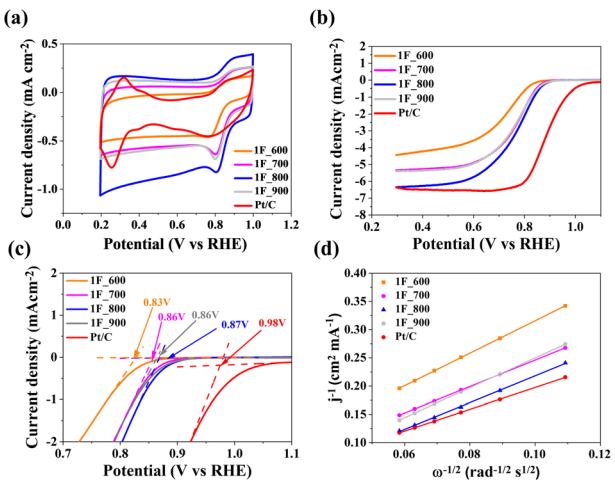

Fig. 4 The results of electrochemical performance for 1F_*T* and Pt/C saturated with O_2 in 0.1 mol L^{-1} KOH (a) CV plots with a scan rate of 10 mV s^{-1}, (b) LSV plots with a scan rate of 5 mV s^{-1} and rotation speed of 1600 rpm, (c) onset potential, (d) Koutecky–Levich plots at 0.5 V *vs.* RHE for samples in the 1F_*T* series.

Table 2 ORR performance parameters of the obtained N-doped graphene foams compared to commercial Pt/C catalyst, tested in 0.1 mol L^{-1} KOH

Catalyst	E_p (V *vs.* RHE)	E_{onset} (V *vs.* RHE)	$E_{1/2}$ (V *vs.* RHE)	Diffusion-limiting current (mA cm^{-2})	*n* (0.5 V)
Pt/C	0.76	0.98	0.88	6.37	4.00
1F_600	0.77	0.83	0.73	3.93	3.16
1F_700	0.80	0.86	0.77	5.16	3.88
1F_800	0.80	0.87	0.77	6.18	3.84
1F_900	0.80	0.86	0.77	5.25	3.44
2F_600	0.75	0.81	0.72	3.44	3.19
2F_700	0.78	0.86	0.75	4.22	3.45
2F_800	0.80	0.88	0.77	5.93	3.99
2F_900	0.82	0.91	0.79	5.80	3.43

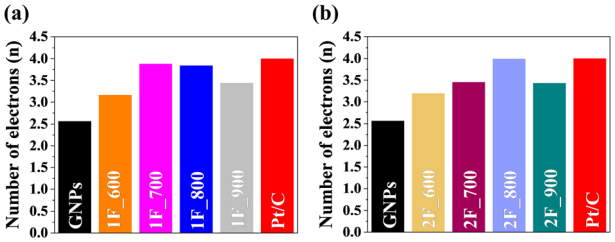

Fig. 5 (a) The number of transferred electrons in the (a) 1F_*T* and (b) 2F_*T* series compared to the commercial catalyst Pt/C and GNPs.

sample 2F_800 is 3.99; this number is equal to the number of electrons transferred for commercial platinum-based carbon.

Conclusions

In summary, the obtained graphene foam electrodes synthesized with natural polymers - gelatine and chitosan are porous and nitrogen-doped. The best graphene-based catalysts are materials carbonized at 800 °C and exhibit a four-electron oxygen reduction pathway in an alkaline medium. The applied carbonization temperatures (up to 800 °C) did not lead to the collapse of the pore structure and the considerable elimination of nitrogen from carbon matrices. The introduction of graphene was seen as an inevitable measure to ensure high electric conductivity of the synthetized ORR catalyst, a key feature for high ORR performance. This plan succeeded, since even carbon matrices obtained at a very low temperature of 600 °C had noticeable values for the number of transferred electrons *n* (3.16 and 3.19). Moreover, the matrices obtained at the highest carbonization temperature of 900 °C did not suffer from diminished structural parameters and exhibited, for example, a surface area above 795 $m^2 g^{-1}$, which is even better than the parameter observed for pristine graphene nanoplatelets. In addition, the influence of quaternary nitrogen functional groups and the predominance of pyridinic groups on the catalytic activity of the obtained materials were investigated. In the future, the presented graphene foams will be successfully used as commercial electrodes for energy storage devices such as metal–air batteries and fuel cells.

Conflicts of interest

There are no conflicts to declare.

Acknowledgements

This work was carried out under research project no. 2019/35/N/ST5/02691, financed by the National Science Centre.

References

1 G. Lemes, D. Sebastián, E. Pastor and M. J. Lázaro, *J. Power Sources*, 2019, **438**, 227036.
2 Y. Shao, Z. Jiang, Q. Zhang and J. Guan, *ChemSusChem*, 2019, **12**, 2133–2146.
3 X. Wen, Z. Duan, L. Bai and J. Guan, *J. Power Sources*, 2019, **431**, 265–273.
4 C. Han and Z. Chen, *Appl. Surf. Sci.*, 2020, **511**, 145382.
5 X. Tong, M. Cherif, G. Zhang, X. Zhan, J. Ma, A. Almesrati, F. Vidal, Y. Song, J. P. Claverie and S. Sun, *ACS Appl. Mater. Interfaces*, 2021, **13**, 30512–30523.
6 J. Jin, F. Pan, L. Jiang, X. Fu, A. Liang, Z. Wei, J. Zhang and G. Sun, *ACS Nano*, 2014, **8**, 3313–3321.
7 X. Zheng, J. Wu, X. Cao, J. Abbott, C. Jin, H. Wang, P. Strasser, R. Yang, X. Chen and G. Wu, *Appl. Catal., B*, 2019, **241**, 442–451.
8 Y. Yan, W. I. Shin, H. Chen, S.-M. Lee, S. Manickam, S. Hanson, H. Zhao, E. Lester, T. Wu and C. H. Pang, *Carbon Lett.*, 2021, **31**, 177–199.
9 Z.-L. Wang, D. Xu, H.-G. Wang, Z. Wu and X.-B. Zhang, *ACS Nano*, 2013, **7**, 2422–2430.
10 D. Su, *Chem. Commun.*, 2012, **48**, 7149–7151.
11 S. P. Patole, S. K. Reddy, A. Schiffer, K. Askar, B. G. Prusty and S. Kumar, *ACS Appl. Nano Mater.*, 2019, **2**, 1402–1411.
12 N. B. Tolou, H. Salimijazi, M. Kharaziha, G. Faggio, R. Chierchia and N. Lisi, *Mater. Sci. Eng. C*, 2021, **126**, 112110.
13 Z. Zhao, H. Wang, H. Huang, L. Li and X. Yu, *Colloids Surf., A*, 2021, **626**, 127125.
14 Y. Zhao, J. Liu, Y. Hu, H. Cheng, C. Hu, C. Jiang, L. Jiang, A. Cao and L. Qu, *Adv. Mater.*, 2013, **25**, 591–595.
15 H. Wu, S. Deng, Y. Shao, J. Yang, X. Qi and Y. Wang, *ACS Appl. Mater. Interfaces*, 2019, **11**, 46851–46863.
16 W. Chen, D. Li, L. Tian, W. Xiang, T. Wang, W. Hu, Y. Hu, S. Chen, J. Chen and Z. Dai, *Green Chem.*, 2018, **20**, 4438–4442.
17 K. t. Kaare, E. Yu, A. Volperts, G. Dobele, A. Zhurinsh, A. Dyck, G. Niaura, L. Tamasauskaite-Tamasiunaite, E. Norkus and M. Andrulevicius, *ACS Omega*, 2020, **5**, 23578–23587.
18 A. Olad and H. B. K. Hagh, *Composites, Part B*, 2019, **162**, 692–702.
19 Y. Dai, W. Li, Z. Chen, X. Zhu, J. Liu, R. Zhao, D. S. Wright, A. Noori, M. F. Mousavi and C. Zhang, *J. Mater. Chem. A*, 2019, **7**, 16397–16405.
20 M. Skorupska, A. Ilnicka and J. P. Lukaszewicz, *Processes*, 2022, **10**, 643.
21 Z. Lin, G. H. Waller, Y. Liu, M. Liu and C.-p. Wong, *Carbon*, 2013, **53**, 130–136.
22 B. Bera, A. Chakraborty, T. Kar, P. Leuaa and M. Neergat, *J. Phys. Chem. C*, 2017, **121**, 20850–20856.
23 J. Guo, S. Zhang, M. Zheng, J. Tang, L. Liu, J. Chen and X. Wang, *Int. J. Hydrogen Energy*, 2020, **45**, 32402–32412.
24 E. S. Cardoso, G. V. Fortunato, I. Palm, E. Kibena-Poldsepp, A. S. Greco, J. L. Junior, A. Kikas, M. Merisalu, V. Kisand and V. Sammelselg, *Electrochim. Acta*, 2020, **344**, 136052.
25 Q. Li, S. Zhang, L. Dai and L.-s. Li, *J. Am. Chem. Soc.*, 2012, **134**, 18932–18935.
26 J. Shui, M. Wang, F. Du and L. Dai, *Sci. Adv.*, 2015, **1**, e1400129.
27 M. M. Rahman, M. Muttakin, A. Pal, A. Z. Shafiullah and B. B. Saha, *Energies*, 2019, **12**, 4565.

28 H. Yang, S. Kou, Z. Li, Z. Chang, M. Wang, Z. Liu and G. Lu, *RSC Adv.*, 2019, **9**, 40301–40308.
29 E. J. Biddinger and U. S. Ozkan, *J. Phys. Chem. C*, 2010, **114**, 15306–15314.
30 H. Lei, M. Cui and Y. Huang, *ACS Appl. Mater. Interfaces*, 2022, **14**, 34793–34801.
31 J. Wu, L. Ma, R. M. Yadav, Y. Yang, X. Zhang, R. Vajtai, J. Lou and P. M. Ajayan, *ACS Appl. Mater. Interfaces*, 2015, **7**, 14763–14769.
32 H. Miao, S. Li, Z. Wang, S. Sun, M. Kuang, Z. Liu and J. Yuan, *Int. J. Hydrogen Energy*, 2017, **42**, 28298–28308.